NATIONAL AERONAUTICS AND SPACE ADMINISTRATION

# Technical Report 32-1298

# Static Aerodynamic Characteristics of Three Blunted Sixty-Degree Half-Angle Cones at Mach Numbers From 0.60 to 1.30

*Wayne J. Marko*
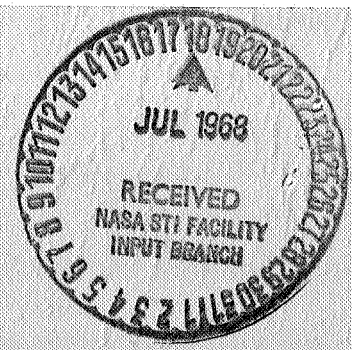
**JET PROPULSION LABORATORY**

CALIFORNIA INSTITUTE OF TECHNOLOGY

PASADENA, CALIFORNIA

July 1, 1968

*Technical Report 32-1298*

# Static Aerodynamic Characteristics of Three Blunted Sixty-Degree Half-Angle Cones at Mach Numbers From 0.60 to 1.30

*Wayne J. Marko*

Approved by:

Bain Dayman, Jr., Manager
Aerodynamics Facilities Section

*TECHNICAL REPORT 32-1298*

# Acknowledgment

The experimental investigation, in which the data reported herein were obtained, was successfully concluded through the cooperation of the NASA Ames Research Center Experimental Investigations Branch. Particular recognition is due Messrs. Russell Fahey and Daniel Petroff, members of the Experimental Investigations Branch staff, for their patient approach to the problems encountered during the test program.

# Contents

## Figures

# Abstract

Static aerodynamic characteristics are presented for three 60-deg half-angle cones tested at transonic speeds. These data, obtained during tests in the NASA Ames Research Center 2 × 2-ft transonic wind tunnel, are compared with JPL data at low supersonic speeds ($M = 2.2$). Base pressures are compared with other JPL data for similar configurations and experimental base pressure data from Sighard F. Horner's *Fluid-Dynamic Drag*. The ranges of model parameters are: nose bluntness (nose radius/base diameter) ratio of 0.10, and edge radius/base diameter ratios of 0.0, 0.05, and 0.10. The test Mach number range was 0.60–1.30. This report is complementary to JPL TR 32-1213, a systematic and more extensive supersonic regime investigation of these and related configurations.

# Static Aerodynamic Characteristics of Three Blunted Sixty-Degree Half-Angle Cones at Mach Numbers From 0.60 to 1.30

## I. Introduction

Interest in unmanned exploration of earth's neighboring planets has generated aerodynamic studies of blunt bodies suitable for atmospheric entry. Early in 1966, the JPL Aerodynamic Facilities Section embarked on a program to investigate the aerodynamic characteristics of blunted conical shapes, both statically and dynamically through the subsonic, transonic, supersonic, and hypersonic speed regimes.

The purpose of this report is to present in summary form* the subsonic–transonic static force and moment data obtained in the NASA Ames Research Center (ARC) 2 × 2-ft transonic wind tunnel through the Mach number range of 0.60–1.30. Tests were performed at one Reynolds number, $0.40 \times 10^6$/in., for an approximate angle of attack range of −8 to +28 deg. This program was a cooperative effort by the JPL Aerodynamic Facilities Section and the

NASA Ames Research Center's Experimental Investigations Branch conducted at the request of JPL.

Data are presented in a summary form that is usually most useful in aerodynamic design exercises. The effects of Mach number and model edge radius are discussed with relation to normal force, axial force, and static stability coefficients. A limited number of shadowgraph photographs are presented to show the flow near the maximum diameter of the models tested. Data from Ref. 1 at $M = 2.2$ are included for comparison with the coefficients presented. Base pressure coefficient data are compared with those of Refs. 2 and 3.

Model configurations (Fig. 1) were three spherically blunted 60-deg half-angle cones, each with a different degree of roundness on the edge (shoulder). The nose radius to model diameter ratio for all three configurations was 0.10, as shown in Fig. 1. The three edge radius to diameter ratios were 0.0, 0.05, and 0.10. These configurations were "sting" mounted, as shown in Fig. 2. Forces and moments were obtained with a JPL internal strain gage balance with the sign convention shown in Fig. 3. This sign convention was used throughout this report.

---

*The complete experimental procedures and results of the transonic experimental program, from which the test data presented herein were obtained, are contained in SR 900-169. This publication is available upon request to J. Jackson, Support Section, Technical Information and Documentation Division, Jet Propulsion Laboratory.

DIMENSIONS ARE IN INCHES

$M_{60} N_{10} E_{00}$          $M_{60} N_{10} E_{05}$          $M_{60} N_{10} E_{10}$
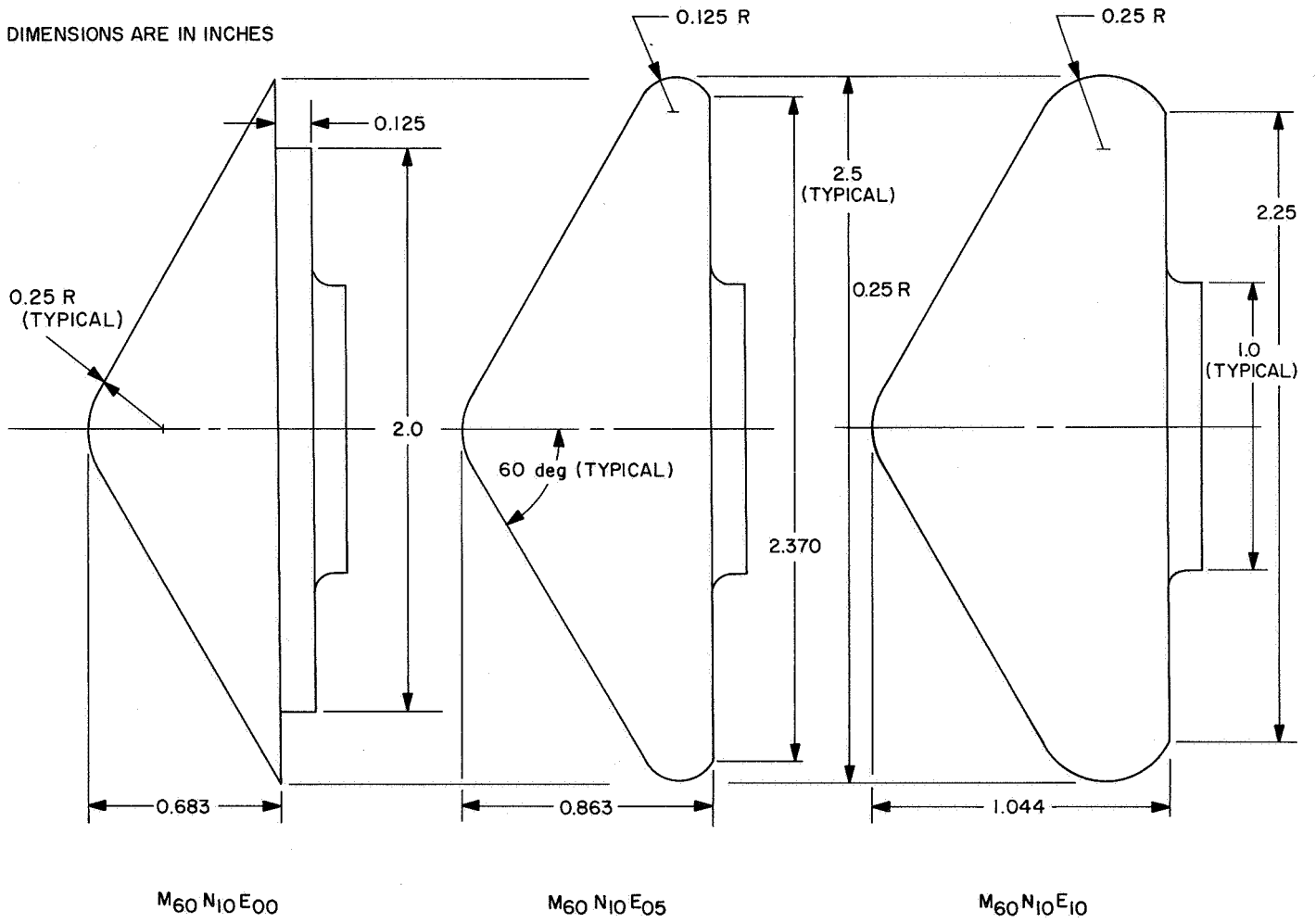
**Fig. 1. Model configurations**
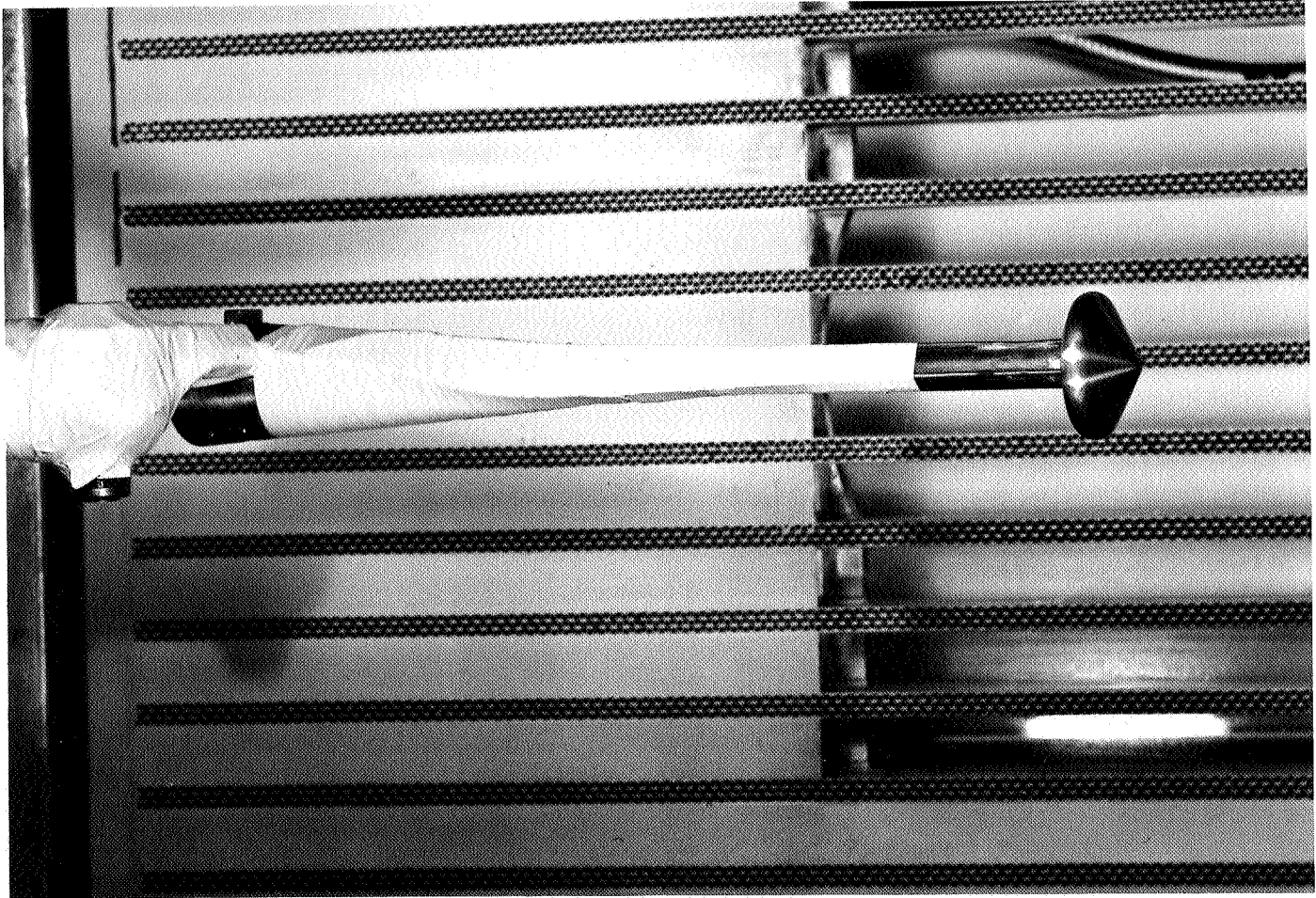
**Fig. 2. Typical model installation in ARC 2 × 2-ft transonic wind tunnel**
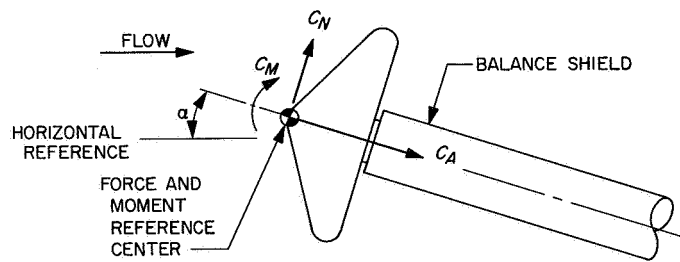


**Fig. 3. Axes system with sign convention**

M = 0.60      M = 1.00      M = 1.30

CONFIGURATION: $M_{60}N_{10}E_{00}$

M = 0.60      M = 1.00      M = 1.30

CONFIGURATION: $M_{60}N_{10}E_{05}$

M = 0.60      M = 1.00      M = 1.30

CONFIGURATION: $M_{60}N_{10}E_{10}$

**Fig. 4. Shadowgraph photographs at $M = 0.60$, 1.00, and 1.30, $\alpha = 0$ deg**

## II. Flow Field Visualization

Shadowgraph pictures of the three configurations at $\alpha = 0$ deg, obtained for Mach numbers 0.60, 1.00, and 1.30, are shown in Fig. 4. These pictures reveal the flow field around the maximum diameter of the models and the near wake characteristics. A bow shock wave is present at $M = 1.30$.

Separation onset, marking the beginnings of a wake, occurs at the sharp edge of configuration $M_{60} N_{10} E_{00}$. However, it is present on the forward face of the configurations $M_{60} N_{10} E_{05}$ and $M_{60} N_{10} E_{10}$, near the point of tangency of the conical face and the edge radius. A small shock wave is present near the point of separation at $M = 1.00$ and 1.30 for these configurations with an edge radius.
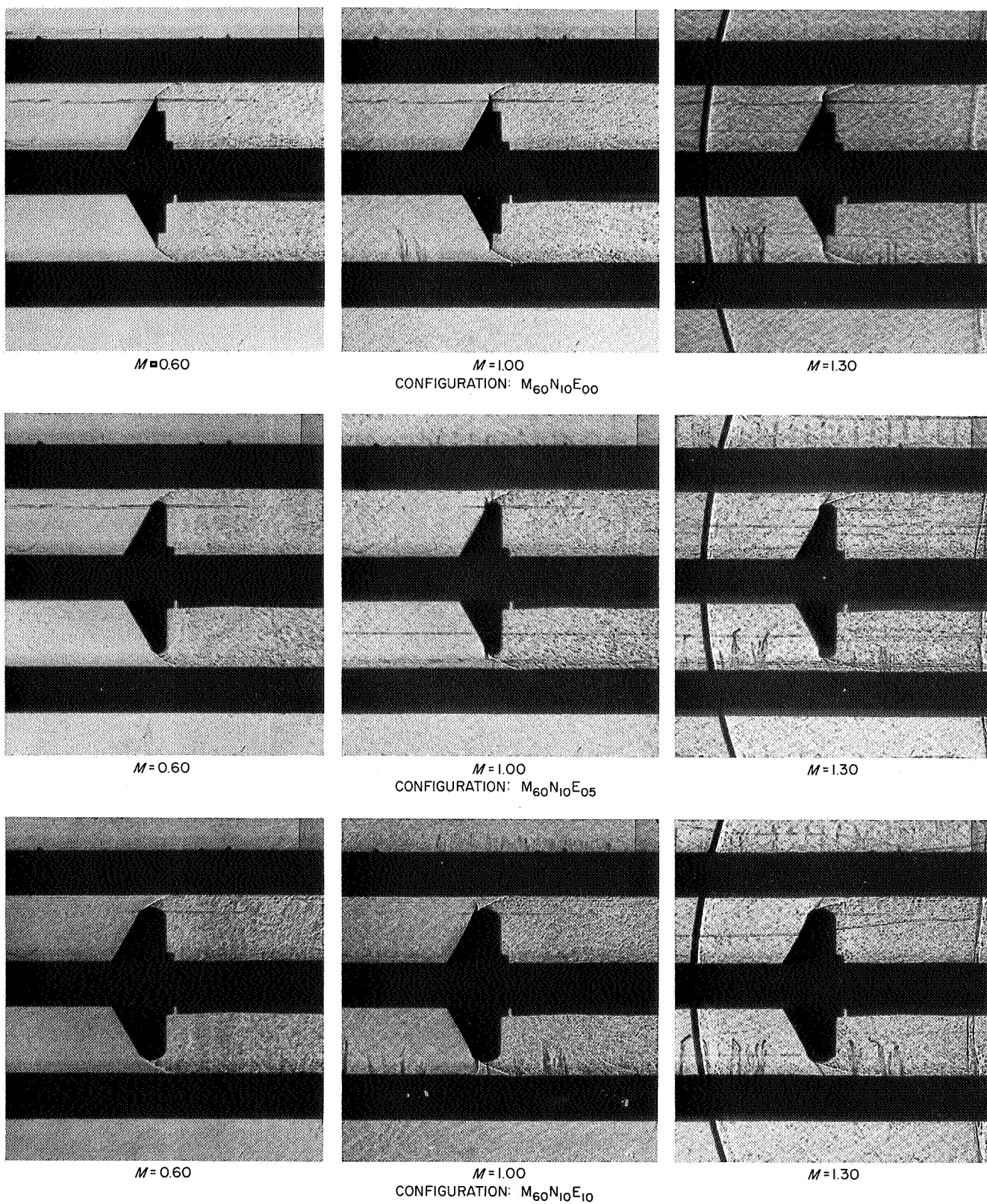
The initial wake angle, the acute angle made with the horizontal, is clearly defined and decreases with increasing Mach number, as expected. The only configuration where the onset of wake turbulence can be seen is $M_{60} N_{10} E_{00}$ at $M = 0.60$. A laminar wake exists downstream from the model for less than ½ of a model diameter before the transition to a turbulent wake occurs. All other wakes appear to be turbulent downstream from the model base.

Optical distortion is evident at $M = 1.00$ and 1.30 in the bow shock wave and at the point of separation. It appears as a thickening of the shock wave and a bubble at the point of separation. The black bars seen in the pictures are tunnel-boundary layer-removal slots that are necessary for transonic tunnel operation. The interaction of the bow shock wave with the tunnel walls is visible at $M = 1.30$, downstream of the model.

## III. Normal Force Coefficient $C_N$

The normal force data, that were obtained in the experimental program, display two anomalies sometimes encountered in wind tunnel tests. First, the normal force curve does not pass through $C_N = 0$ at $\alpha = 0$. Second, the data, obtained with two sting arrangements designed to extend the available angle of attack range, do not always match up. The solution to the problem has been to generate new data in the following manner. Data obtained with a low angle of attack sting were shifted a constant amount, either positive or negative equal to the offset observed in the test data at $\alpha = 0$. Examination of the data obtained with the high angle of attack sting revealed that the slope $C_N$ was fairly linear and, in most instances,

equal to the normal force curve slope of the data obtained with a low angle of attack sting at $\alpha = 13$–15 deg, the overlap attitude range. The normal force curves resulting from these data shifts for the three configurations tested are shown in Fig. 5. The data are essentially linear at angles of attack greater than 12 deg.

A typical presentation for normal force coefficient cross plots is $C_{N_\alpha}$, the normal force curve slope (since reconstruction of $C_N$ is quickly available from $C_{N_\alpha}$). However, reasonable linearity of the data over the angle of attack range are required for this method of presentation. As previously mentioned, the data presented here are not linear; therefore, $C_N$ at discrete angles of attack has been presented rather than the normal force curve slope.

### A. Effect of Mach Number

The effects of Mach number for the three configurations are shown in Fig. 6 for several angles of attack.

Several trends in the data can be observed. $C_N$ is relatively insensitive to Mach number effects at angles of attack below 8 deg. A decrease in normal force is indicated at the transonic speed range, $M = 0.8$ to 1.2, with a plateau suggested for the supersonic speed range (a characteristic indicated in Ref. 1). Data from this reference support the levels obtained here at $M = 1.3$.

Accurate correlation of these data with flow visualization photographs from additional tests might show some relationship between the point of flow separation and the Mach number and the angle of attack effects. It should be noted that the most distinct changes in normal force occur for those Mach numbers where the wake begins to converge (close).

### B. Effect of Edge Radius

Up to $\alpha = 28$ deg (the maximum $\alpha$ investigated), normal force is not particularly affected by edge radius for $R_E/D < 0.05$, as shown in Fig. 7. In addition, normal force is relatively insensitive to edge radius changes for angles of attack below 16 deg. Normal force data for a 60-deg half-angle cone of any edge radius within the range tested may be conveniently determined.

## IV. Axial Force Coefficient $C_A$

Two interesting characteristics were present in the axial force data obtained in the experimental program. An unexpected increase occurred in $C_A$ as $\alpha$ increased from 0 to 4 deg and in the offset at the overlap of the data
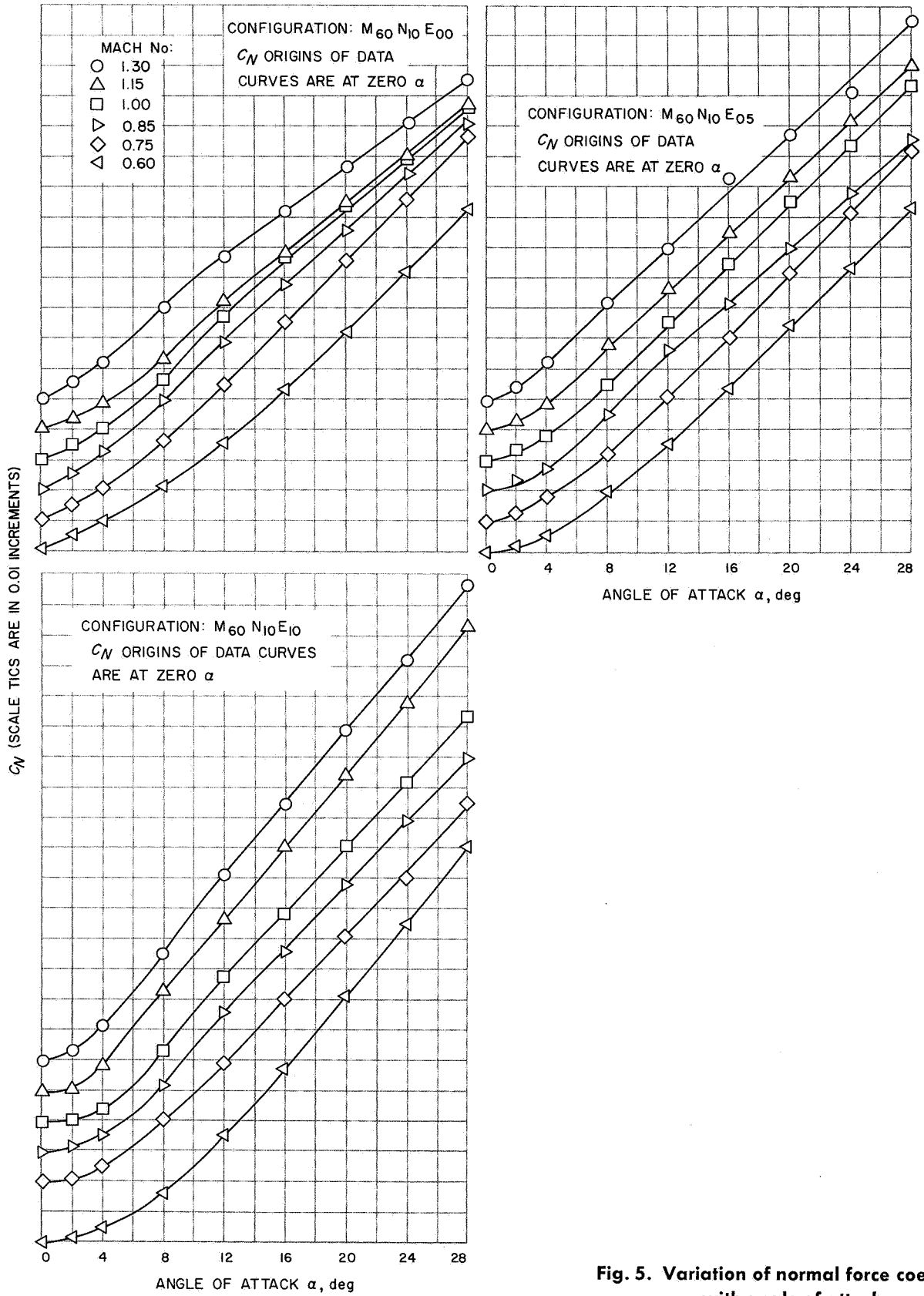
Fig. 5. Variation of normal force coefficient
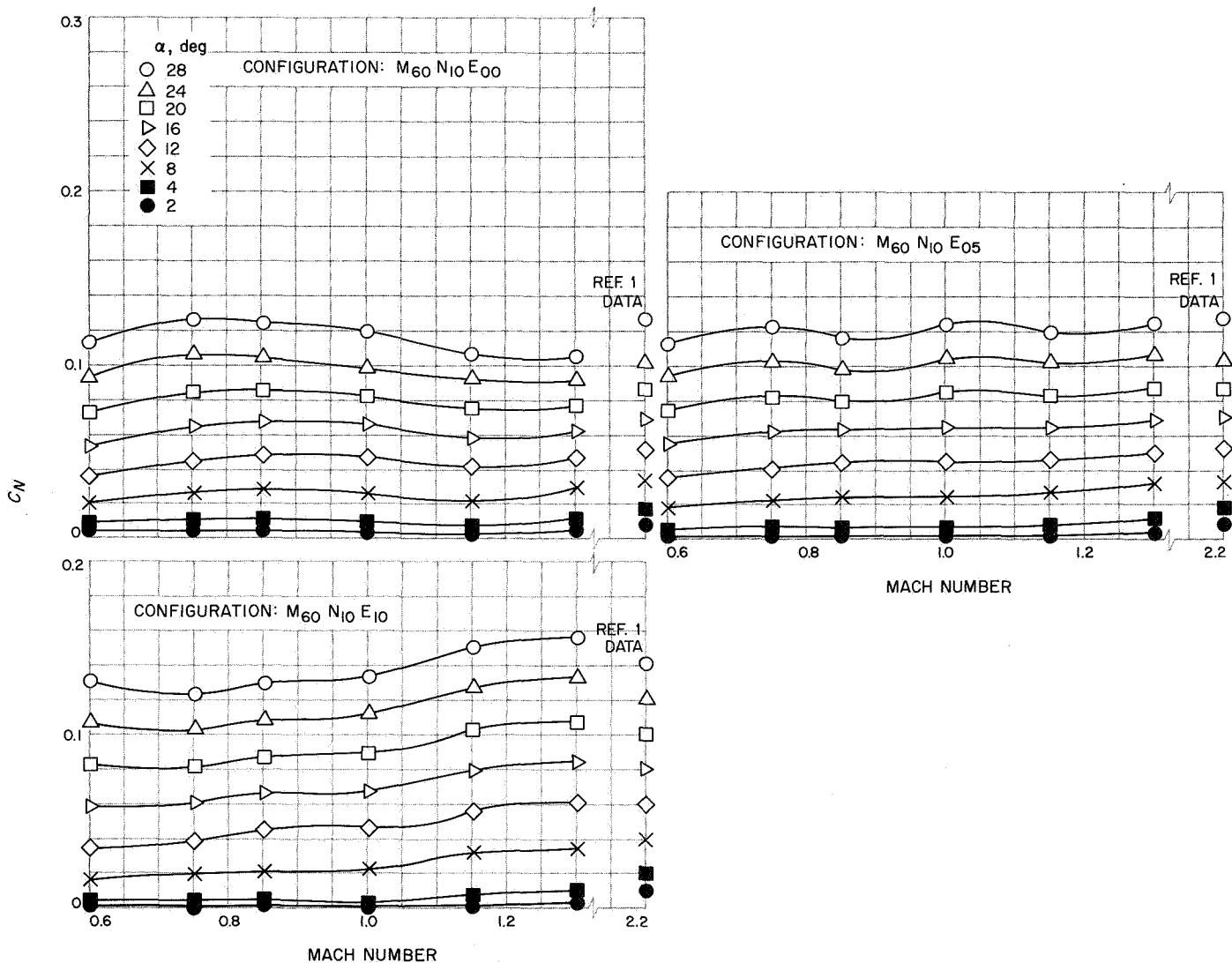with angle of attack

**Fig. 6. Variation of normal force with Mach number for discrete angles of attack**

resulting from the use of two different sting configurations. This increase in $C_A$ within the angle of attack range of 0–4 deg was also observed in the supersonic regime data of Ref. 1. However, an examination of the axial force data curve as a whole indicated that a problem such as aerodynamic interference may exist at angles of attack greater than 4 deg.

Experience with free-flight dynamic stability studies at JPL for the supersonic speed regime has established that a satisfactory form for the curve-fit equation to either the drag or axial force data of conical bodies may be fourth-order polynomial for low amplitudes ($\alpha < 30$ deg). A quick test curve fit to the original test data showed that this approximation was not satisfactory. As a result, the forebody axial force characteristics were examined by

subtracting the base pressure contribution from the total axial force, using the base pressure obtained in the test. This coefficient was based on the data reduction reference area A. The resulting curves did fit the fourth-order polynomial approximation and, in addition, the sting induced offset was significantly reduced. The results of this reconstruction of forebody axial force are presented in Fig. 8.

## A. Variation With Mach Number

The data in Fig. 8 have been crossplotted in summary form at zero angle of attack. The effect of Mach number on $C_A$ at $\alpha = 0$ is shown in Fig. 9.
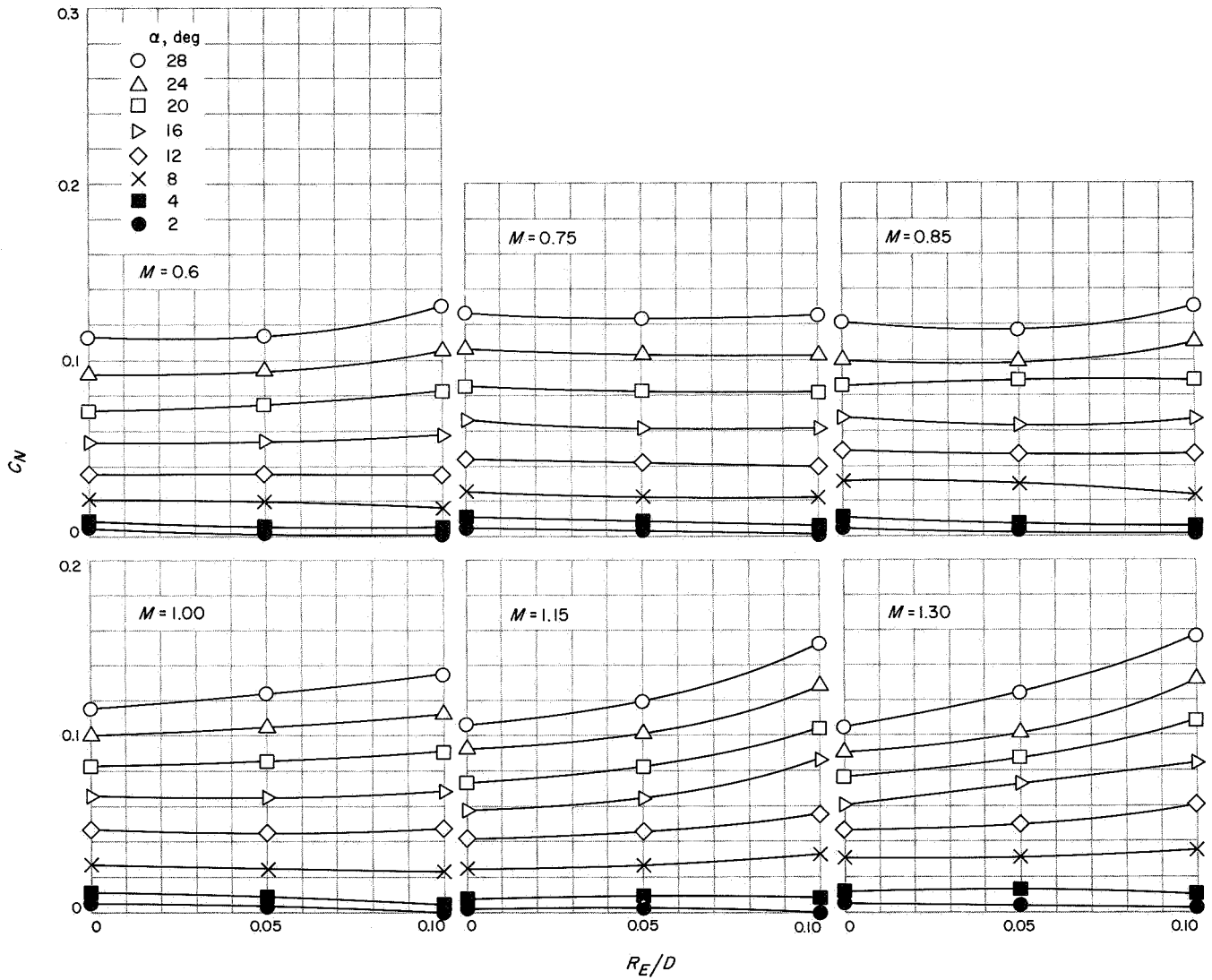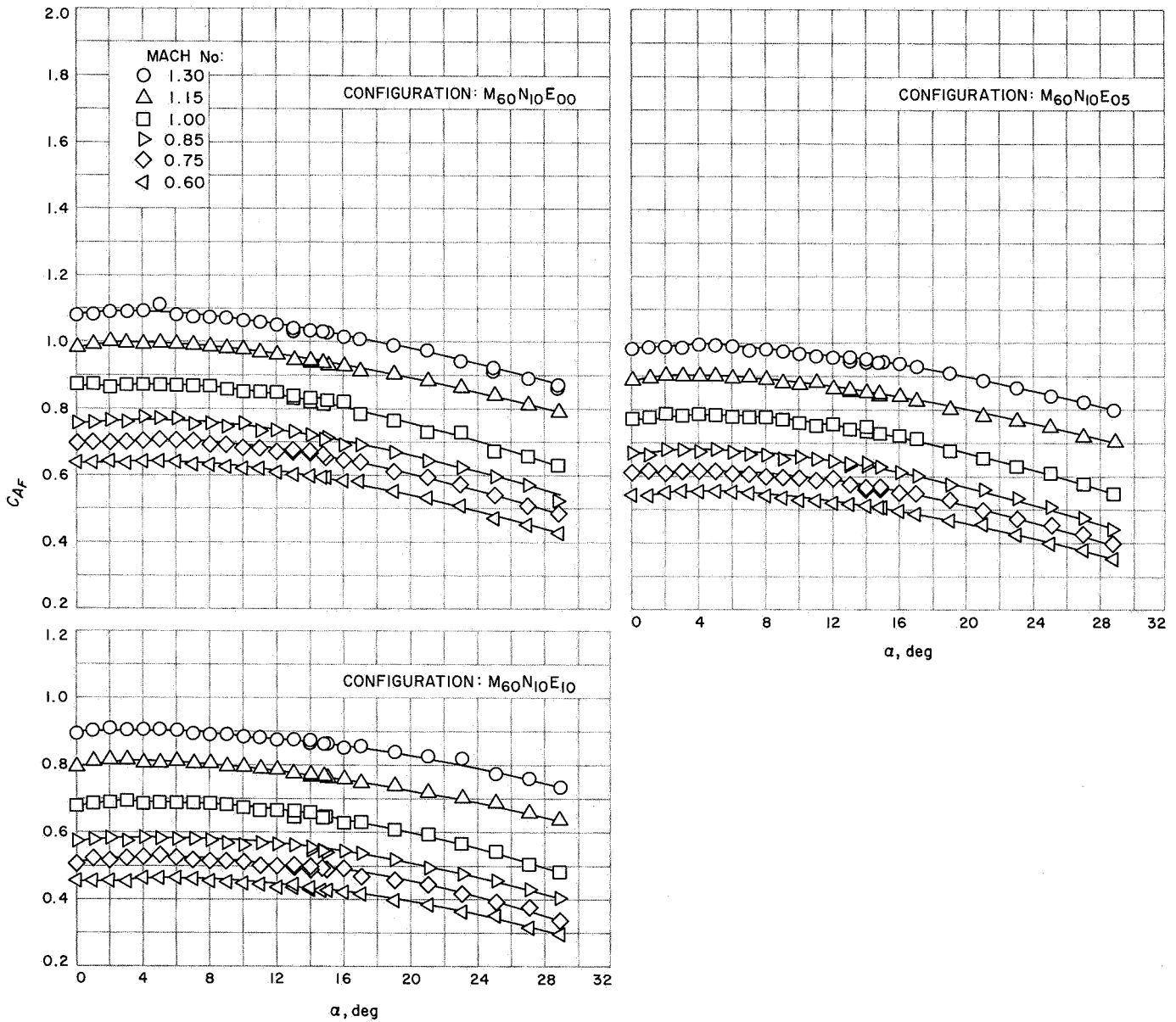
Fig. 7. Effect of edge radius on normal force coefficient

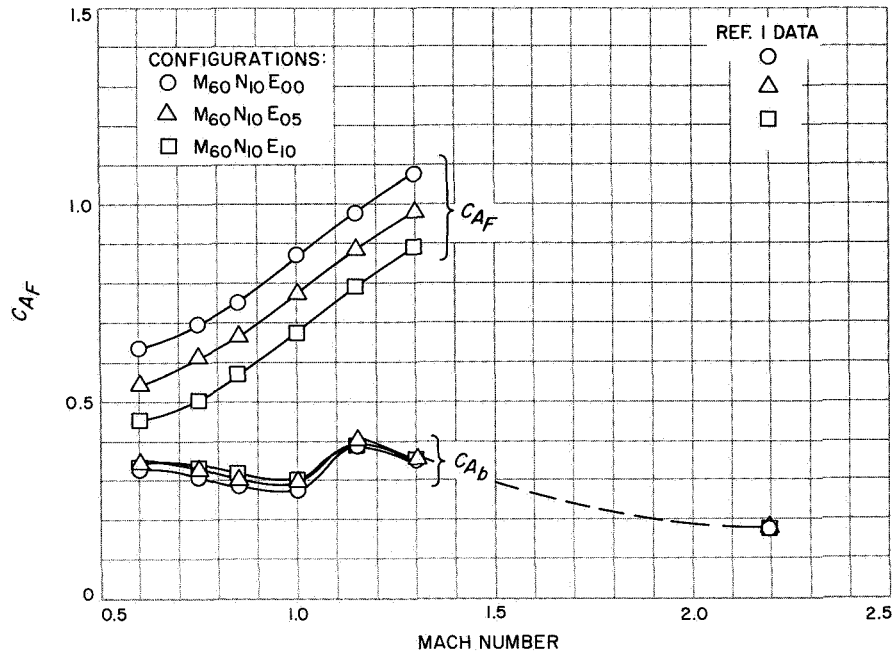Fig. 8. Variation of axial force coefficient with angle of attack

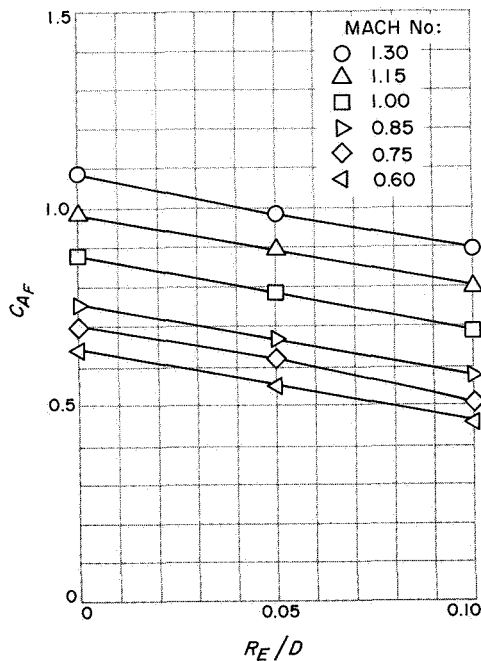**Fig. 9. Effect of Mach number on axial force, $\alpha = 0$ deg**



**Fig. 10. Variation of axial force with edge radius, $\alpha = 0$ deg**

Axial force rise in the transonic speed regime is similar for each configuration, although each curve is at a discrete level with drag decreasing with increasing edge radius. Axial force due to base pressure is shown below

the forebody axial force curves. Differences between the data configurations are slight in the transonic regime and almost non-existent at $M = 0.6$ and 1.30. The general trends in base pressure drag are similar to those reported for spheres (Ref. 3). A total axial force coefficient may be obtained by adding the forebody and axial force coefficients. Coefficient levels cited in Ref. 1 at $M = 2.2$ are also shown with the axial force due to base pressure subtracted from the total axial force.

### B. Variation With Edge Radius

No surprises are evident in the effect of edge radius as shown in Fig. 10. The axial force decreases linearly with increasing edge radius for all but two Mach numbers: 0.75 and 1.30. However, these deviations from the linear case are small. Axial force for any 60-deg cone and edge radius at $\alpha = 0$ may be easily estimated for $R_E/D < 0.1$.

### V. Base Pressure Coefficient $C_{P_b}$

Base drag of various simple projectile and missile body shapes have received much attention in recent years as evident in Ref. 3. However, a fundamental or all encompassing solution has not been found to the base flow problem, and the aerodynamicist is left with the task of cataloging experimental material over the Mach number range of interest for desired configurations. The

majority of base pressure data are obtained with sting mounted models, and it must be acknowledged that the presence of a sting may influence these data. Base pressure data obtained from configurations in free-flight would virtually eliminate this question of data accuracy.

Reference 3 catalogues a large number of base pressure data. The majority of shapes are slender and do not present the same flow picture as that of the 60-deg half-angle cone. However, some data trends are similar to those of the 60-deg half-angle cone and are, therefore, considered worthy of mention. Trends in these base pressure coefficients for a slender body in the transonic speed regime (Ref. 3) show an increase in coefficient at low transonic Mach numbers $(M = 0.8)$. This coefficient becomes a maximum near $M = 1.0$. A slight decrease in base pressure coefficient is observed at $M > 1.0$, and then a constant level occurs between $M = 1.5$ and 2.5, whereafter the wake closes and the data follow the supersonic base pressure curve.

The data obtained in this experiment can be compared with the aforementioned data, but only in a general manner since there are definite differences between the configurations. The measured base pressure decreases to a minimum at $M = 1.0$, as shown in Fig. 11, followed by a rapid rise and peak at $M = 1.15$. No constant low supersonic $(M = 1.5–2.5)$, base pressure coefficient (as shown in Ref. 3) is observed; this deviation from the reference data may be the result of the high initial subsonic-transonic base pressure coefficient registered for these configurations. The sharp decreases in base pressure at

$M = 1.3$ are accompanied by a decrease in the cone wake angle apparent in the shadowgraph photos.

The data shown in Fig. 11 are in good agreement with the supersonic data of Refs. 1 and 2 if extrapolated at supersonic speeds. However, the correlation function $1/M^2$ is not useful in predicting base pressure for $M < 2$. The supersonic base pressure data curve (Ref. 3) reasonably approximates the supersonic data trends indicated by this study.

## VI. Static Stability, Center-of-Pressure Location $X_{cp}/D$

The location of the center-of-pressure is an established measure of the static stability of a vehicle in flight. A center-of-pressure located aft from the vehicle center of gravity assures that a restoring moment exists when the vehicle is disturbed from a trim condition. This parameter is, of course, important. However, the vehicle dynamic damping characteristics must also be considered in the final examination of inflight stability.

The $C_M$ vs $C_N$ data were nonlinear, especially at angles of attack less than 8 deg. The slope, $\partial C_M/\partial C_N$, which was synonymous with the center-of-pressure, was therefore nonlinear. As a result, $X_{cp}/D$ was determined at several discrete angles of attack (0, 4, 8, and 20–28 deg). Data trends should be clear with this method of presentation. The center-of-pressure was measured aft (negative) from the physical nose of the configuration.
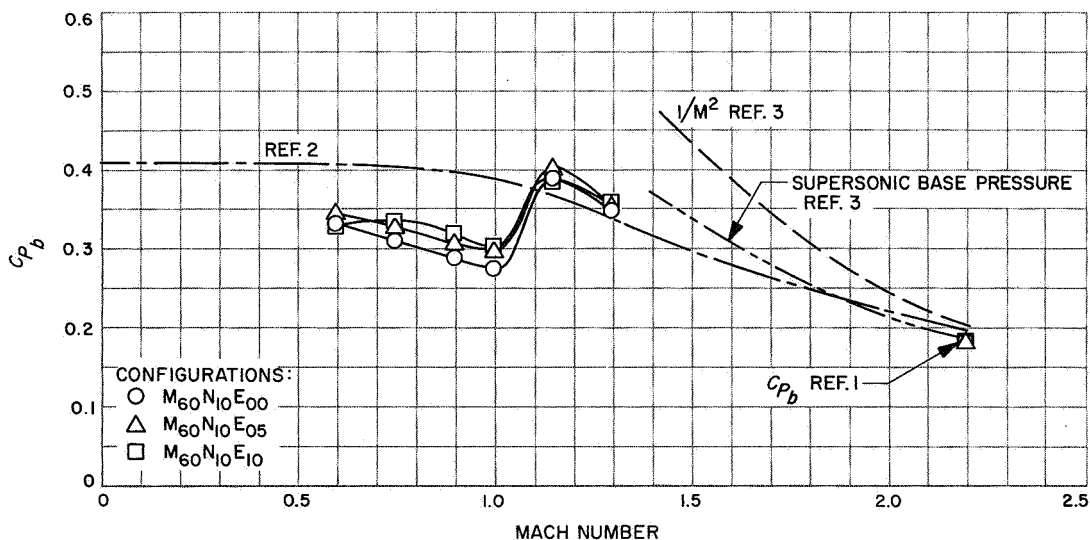


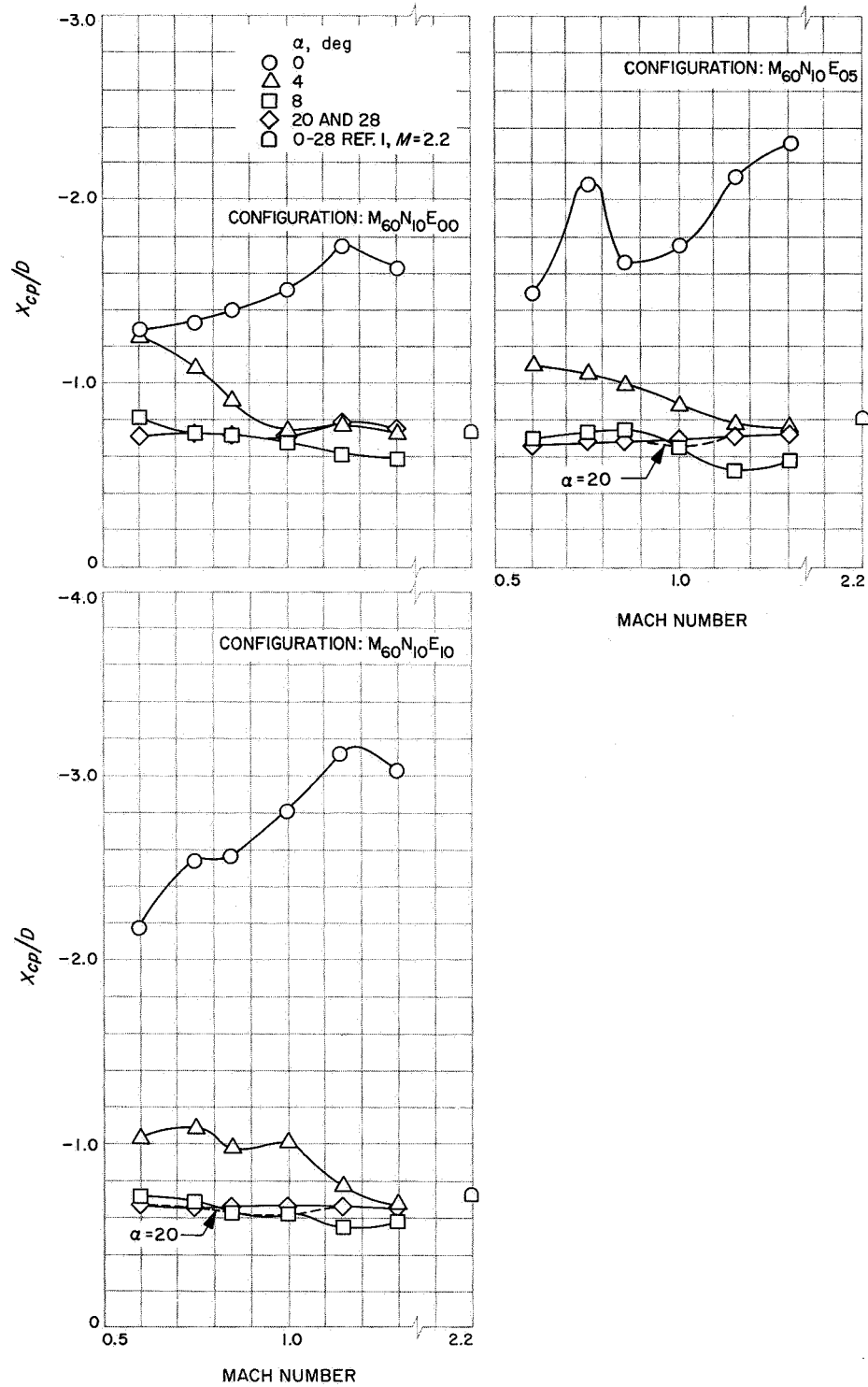Fig. 11. Variation of base pressure with Mach number, $\alpha = 0$ deg

Fig. 12. Variation of center-of-pressure location with Mach number

## A. Variation With Mach Number

The effect of Mach number on the center-of-pressure location at the chosen angles of attack is presented in Fig. 12 for the three configurations tested. The center-of-pressure is aft of the base for all three configurations and moves further aft with increasing Mach number at or near $\alpha = 0$ deg. Increasing the angle of attack reduces stability, since the center-of-pressure moves forward. However, the center-of-pressure is always aft of the physical body. Center-of-pressure location for angles of attack greater than 8 deg is relatively invariant with increasing Mach number.

## B. Variation of Edge Radius

The importance of the edge radius on static stability at or near $\alpha = 0$ deg is clearly demonstrated in Fig. 13a. Significant gains in static stability margin can be obtained by increasing the value $R_E/D$ at all the Mach numbers tested. This edge radius dependence at higher angles of attack (4–28 deg), presented in Figs. 13 b–d, is significantly diminished. For the angle of attack range of 20–28 deg, the dependence of $X_{cp}/D$ on edge radius is shown as a slightly decreasing static stability with increasing edge radius. The Mach number dependence of $X_{cp}/D$ at high angles of attack is negligible.
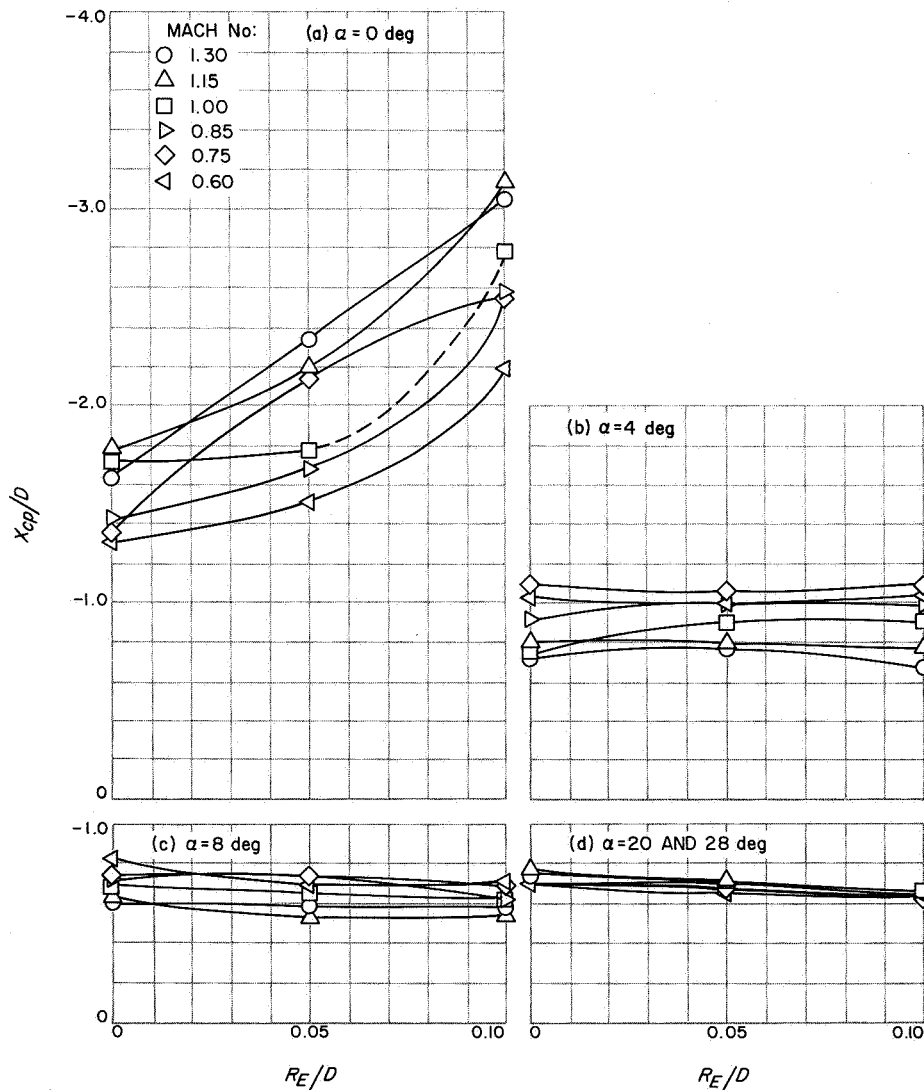


Fig. 13. Variation of center-of-pressure location with edge radius

Data for $M = 1.0$ at $R_E/D = 0$, and $\alpha = 0$ do not follow the trends established by other data at this edge radius/diameter ratio. More data would be useful in assessing the accuracy of the results in this angle of attack range. Similarly, data for $M = 0.75$ at $R_E/D = 0.05$ and $\alpha = 0$ do not follow the trends indicated by the $M = 0.60$ and 0.85 data.

## VII. Concluding Remarks

The following conclusions and remarks are presented for this study.

(1) Normal force coefficient $C_N$ is generally well behaved with Mach number and is consistent with data at $M = 2.2$ (Ref. 1). Edge radius variation produces minimal effects on $C_N$ for $R_E/D \leq 0.05$ and all edge radii investigated for $\alpha < 8$ deg.

(2) Forebody axial force increases smoothly with Mach number and decreases (almost linearly) with increasing edge radius.

(3) Base pressure coefficient ($\alpha = 0$ deg) agrees well with those of Refs. 1 and 2 for $M > 1$. Trends for $M \leq 1$ are similar to those reported for more slender bodies (Ref. 3). No base pressure data at angle of attack are presented because of suspected support interference.

(4) The configurations are longitudinally statically stable for all Mach numbers and angles of attack. In fact, the center-of-pressure is always located aft of the physical dimensions of the configuration for the full range of test parameters. Static stability decreases with increasing angle of attack and approaches, at $M = 1.3$, the stability shown in Ref. 1 at $M = 2.2$, except for configuration $M_{60} N_{10} E_{10}$, which possesses more static stability at $M = 1.3$ than that indicated at $M = 2.2$ (Ref. 1).

(5) Slight decreases in static stability with increasing edge radius are indicated for the angle of attack range of 20–28 deg.

(6) A preliminary comparison of the data described herein with those of Ref. 1 has shown that they are consistent with each other over the subsonic-transonic-supersonic speed regimes. An in-depth comparison has not been included since it does not lie within the scope of this report.

## Nomenclature

$A$    reference area $= \pi D^2/4$, (4.909 in.$^2$)

$C_{A_b}$    axial force coefficient due to differential between base pressure and free stream static pressure $= (P_b - P_\infty) A/qA$

$C_{A_F}$    forebody axial force coefficient $=$ (axial force$/qA$) $+ (P_b - P_\infty)/q$

$C_M$    pitching moment coefficient referenced to the physical model nose $=$ (pitching moment$/qAD$)

$C_N$    normal force coefficient $=$ (normal force$/qA$)

$C_{P_b}$    base pressure coefficient $= (P_b - P_\infty)/q$

$D$    model maximum diameter

$M$    Mach number

$P_\infty$    freestream static pressure

$P_b$    base pressure

$q$    dynamic pressure $= \frac{1}{2} \rho V^2$

$Re$    Reynolds number

$R_E$    model edge (shoulder) radius

$R_N$    model nose radius

$X_{cp}$    center-of-pressure location measured from the physical nose, negative aft

$\alpha$    angle of attack

Configuration:

$M_{(--)}$    cone half-angle of (--) deg

$N_{(--)}$    nose radius of (--)% of model diameter

$E_{(--)}$    edge radius of (--)% of model diameter

# References

1. Walker, B., and Weaver, R. W., *Static Aerodynamic Characteristics of Blunted Cones in the Mach Number Range From 2.2 to 9.5*, Technical Report 32-1213, Jet Propulsion Laboratory, Pasadena, Calif., Dec. 1, 1967.

2. Nichols, J. O., and Nierengarten, E. A., *Aerodynamic Characteristics of Blunt Cones*, Technical Report 32-677, Jet Propulsion Laboratory, Pasadena, Calif., Nov. 19, 1964.

3. Horner, S. F., *Fluid-Dynamic Drag*, pp. 16-4 and 16-5. Published by the author, Midland Park, New Jersey, 1965.